Indian Ocean Dipole Response to Global Warming: Analysis of Ocean–Atmospheric Feedbacks in a Coupled Model*

XIAO-TONG ZHENG

Physical Oceanography Laboratory and Ocean–Atmosphere Interaction and Climate Laboratory, Ocean University of China, Qingdao, China

SHANG-PING XIE

International Pacific Research Center and Department of Meteorology, School of Ocean and Earth Science and Technology, University of Hawaii at Manoa, Honolulu, Hawaii

GABRIEL A. VECCHI

NOAA/Geophysical Fluid Dynamics Laboratory, Princeton, New Jersey

QINYU LIU

Physical Oceanography Laboratory and Ocean–Atmosphere Interaction and Climate Laboratory, Ocean University of China, Qingdao, China

JAN HAFNER

International Pacific Research Center and Department of Meteorology, School of Ocean and Earth Science and Technology, University of Hawaii at Manoa, Honolulu, Hawaii

(Manuscript received 1 July 2009, in final form 16 September 2009)

ABSTRACT

Low-frequency modulation and change under global warming of the Indian Ocean dipole (IOD) mode are investigated with a pair of multicentury integrations of a coupled ocean–atmosphere general circulation model: one under constant climate forcing and one forced by increasing greenhouse gas concentrations. In the unforced simulation, there is significant decadal and multidecadal modulation of the IOD variance. The mean thermocline depth in the eastern equatorial Indian Ocean (EEIO) is important for the slow modulation, skewness, and ENSO correlation of the IOD. With a shoaling (deepening) of the EEIO thermocline, the thermocline feedback strengthens, and this leads to an increase in IOD variance, a reduction of the negative skewness of the IOD, and a weakening of the IOD–ENSO correlation.

In response to increasing greenhouse gases, a weakening of the Walker circulation leads to easterly wind anomalies in the equatorial Indian Ocean; the oceanic response to weakened circulation is a thermocline shoaling in the EEIO. Under greenhouse forcing, the thermocline feedback intensifies, but surprisingly IOD variance does not. The zonal wind anomalies associated with IOD are found to weaken, likely due to increased static stability of the troposphere from global warming. Linear model experiments confirm this stability effect to reduce circulation response to a sea surface temperature dipole. The opposing changes in thermocline and atmospheric feedbacks result in little change in IOD variance, but the shoaling thermocline weakens IOD skewness. Little change under global warming in IOD variance in the model suggests that the apparent intensification of IOD activity during recent decades is likely part of natural, chaotic modulation of the ocean–atmosphere system or the response to nongreenhouse gas radiative changes.

* International Pacific Research Center Publication Number 638 and School of Ocean and Earth Science and Technology Publication Number 7821.

Corresponding author address: Xiao-Tong Zheng, College of Physical and Environmental Oceanography, Ocean University of China, Qingdao, 266100, China.
E-mail: xzheng@hawaii.edu

DOI: 10.1175/2009JCLI3326.1

1. Introduction

The Indian Ocean dipole (IOD) is a mode of interannual variability over the tropical Indian Ocean that involves ocean–atmosphere interaction in the zonal direction (Saji et al. 1999; Webster et al. 1999; Murtugudde et al. 2000). In a typical IOD event, negative anomalies of sea surface temperature (SST) appear in the southeast equatorial Indian Ocean, with weak positive anomalies in the western part of the basin. By affecting atmospheric convection, the IOD exerts considerable influences on climate both locally and in remote regions. Yamagata et al. (2004), Chang et al. (2006), and Schott et al. (2009) review Indian Ocean climate variability and discuss its phenomenology, dynamics, and predictability.

An east − west SST difference in the Indian Ocean is an often-used IOD index (e.g., Saji et al. 1999; Ashok et al. 2004; Song et al. 2007a), although the largest SST anomalies and the most active ocean–atmosphere coupling occur in the eastern part of the Indian Ocean basin (e.g., Annamalai et al. 2005). In addition to its interannual variations, the IOD exhibits variability on decadal and multidecadal time scales. Ashok et al. (2004) noted low-frequency (8–25 yr) variations in such an IOD index and showed that they are highly correlated with the thermocline depth in the Indian Ocean, a result suggesting the importance of ocean dynamical changes for decadal IOD. Using a high-resolution coupled model, Tozuka et al. (2007) interpreted the decadal IOD as decadal modulation of interannual IOD events through asymmetric occurrence of positive and negative events. IOD activity as measured by frequency of occurrence or variance also displays considerable decadal and longer term variations (Ihara et al. 2008). Based on ocean model experiments, Annamalai et al. (2005) indicated that the shallow thermocline in the eastern equatorial Indian Ocean (EEIO) is important for the development of strong IOD events. Song et al. (2007a) interpreted the statistics of decadal variability the IOD in the Geophysical Fluid Dynamics Laboratory Climate Model version 2.1 (GFDL CM2.1) coupled general circulation model as consistent with chaotic variability, without the need for an underlying oscillation; Song et al. (2007b) found that an EEIO thermocline shoaling resulting from the closure of the Indonesian Throughflow in the GFDL CM2.1 model resulted in a large enhancement of IOD variability. As a recent example of decadal modulation, two consecutive positive IOD events took place in 2006 and 2007 with El Niño and La Niña in the Pacific, respectively (Behera et al. 2008; Luo et al. 2008). Other epochs of strong IOD activity include the 1950s, early 1960s, and 1990s. Epochs of weak IOD activity are the 1970s and 1980s.

Climate change in response to radiative forcing by increasing greenhouse gas (GHG) concentrations could influence IOD properties such as the amplitude and frequency of occurrence. There are many studies of the response of El Niño–Southern Oscillation (ENSO) to global warming (Meehl et al. 1993; Knutson et al. 1997; Timmermann et al. 1999; Fedorov and Philander 2000; Collins 2005; van Oldenborgh et al. 2005; Capotondi et al. 2006; An et al. 2008), but considerable uncertainties remain in model response (Guilyardi et al. 2009). Several recent studies examine Indian Ocean changes in response to global warming. In particular, the thermocline appears to shoal in the EEIO from limited observations for the past ~50 years (Alory et al. 2007), a change that is often seen in global warming model simulations (Vecchi and Soden 2007a; Du and Xie 2008) and results from the weakened Walker circulation. Some studies (Vecchi and Soden 2007a; Ihara et al. 2008) hypothesize that the thermocline shoaling in the EEIO, by enhancing thermocline feedback, could strengthen IOD events in the future. Based on coral oxygen-isotope records, Abram et al. (2008) reported indications of an intensification of IOD activity for the recent 150 years, a period during which atmospheric greenhouse gas concentrations have been increasing steadily. Peculiarly, however, IOD variance changes little in most global warming simulations (Ihara et al. 2009) despite a pronounced shoaling of the EEIO thermocline (Vecchi and Soden 2007a; Du and Xie 2008). This apparent paradox is the focus of this paper.

The present study examines the multidecadal modulation of the IOD and its change under global warming, using a state-of-the-art coupled general circulation model (CGCM) that realistically simulates IOD. We develop a method to evaluate ocean–atmospheric feedback based on regression analysis. This feedback analysis is applied to a long unforced control run and a global warming run forced by increasing GHG. We show that, under global warming, the thermocline shoaling in the EEIO indeed leads to a strengthening of thermocline feedback, but this effect on the IOD is countered by a decrease in atmospheric feedback.

The rest of the paper is organized as follows. Section 2 describes the model and simulations. Section 3 analyzes the long control run and investigates the multidecadal modulation of the IOD in the model. Section 4 examines changes of the Indian Ocean–atmosphere system in global warming and investigates why IOD activity does not intensify in a warmer climate. Section 5 discusses IOD skewness and its response to global warming. Section 6 is a summary.

2. Model and simulations

This study uses the outputs from GFDL CM2.1, a global coupled ocean–atmosphere–land–ice model. The

model formulation and simulation are documented in Delworth et al. (2006). The atmospheric component of the coupled model is the GFDL atmosphere model version 2.1 (AM2.1) (GFDL Global Atmospheric Model Development Team 2004). The model uses a finite-volume dynamical core (Lin 2004), with 2.5° × 2° horizontal resolution and 24 vertical layers. The oceanic component of the model is based on the Modular Ocean Model version 4 (MOM4) code (Griffies et al. 2003), which has a horizontal resolution of 1° × 1° and 50 vertical layers. In the meridional direction the resolution increases toward the equator to 1/3° between 30°S and 30°N. Two climate model (CM) simulations are used in our study: a 500-yr-long ''control run'' under constant radiative forcing in 1860 (see Table 1 of Delworth et al. 2006) and a 440-yr-long ''global warming run.'' The latter is made up of two sections, both from the World Climate Research Program (WCRP) Third Coupled Model Intercomparison Project (CMIP3): a 140-yr-long, climate of the twentieth-century run (20C3M) forced by historical GHG from 1861 to 2000, and a 300-yr projection under the Special Report on Emissions Scenarios A1B (A1B) with a 720-ppm CO_2 stabilization experiment. The initial conditions for the A1B experiment are taken from 1 January 2001 of the 20C3M experiment. We combine the two experiments to form a 440-yr-long dataset and examine the IOD response to global warming.

This study focuses on changes in interannual variability. We perform a three-month running average to reduce intraseasonal variability and calculate a 9-yr running mean to remove decadal and longer variations, which are significant over the tropical Indian Ocean (Deser et al. 2004) in the control and global warming runs. To examine multidecadal modulations of interannual IOD variability, interannual variance is calculated in 50-yr sliding windows at 10-yr intervals (i.e., years 1–50, 11–60, so on).

A linear baroclinic model (LBM) is also used to explore atmospheric dynamics. This model is linearized around the September mean state as represented by the GFDL CM2.1 output. A detailed description of the linear model may be found in Watanabe and Kimoto (2000). We use a version with T42 resolution in the horizontal and 20 sigma levels in the vertical.

3. Multidecadal variability of the IOD in the unforced simulation

The CM2.1 model simulates the climatology and interannual variability of the tropical Indian Ocean (TIO) well (Song et al. 2007a), although the simulated ENSO events are too strong in equatorial SST variability compared to observations (Wittenberg et al. 2006). We have performed an empirical orthogonal function analysis, and Fig. 1 shows the leading modes of interannual SST variability over the TIO based on the 500-yr-long control run[1] with the CO_2 level of year 1860. The first EOF mode, explaining 40% of SST variance, exhibits a basinwide warming. Previous studies (Klein et al. 1999; Du et al. 2009) reported that this mode is a result of ENSO forcing. Its correlation with the Niño-3.4 SST index peaks when the basin mode lags by 4 months in the model. The enhanced warming in the southwest TIO is due to ocean Rossby wave propagation over the thermocline ridge (Xie et al. 2002). The second EOF mode, explaining 18% of SST variance, exhibits an east–west dipole pattern with easterly wind anomalies along the equator. The maximum negative SST anomalies are located along the Java–Sumatra coasts where the wind-forced upwelling occurs during June–October. The EOF results are similar to those of Song et al. (2007a) and comparable with observations.

In addition to the spatial patterns, the model captures the IOD seasonality quite well. Figure 2 shows monthly standard deviations of SST, precipitation, and sea surface height (SSH) in the EEIO (10°S-0°, 90°–110°E), all displaying pronounced seasonality. SST and precipitation variances are strong from August to October, one month earlier than in observations. The peak of SSH variance lags by 2–3 months in November–December, a time delay due to equatorial wave propagation (Yuan and Han 2006). In this paper, we use the standard deviation of SST variability in the EEIO averaged during August–October [ASON; $\sigma(T)$] to represent IOD intensity. EEIO SST variability during ASON is strongly affected by ocean upwelling and thermocline feedback. EEIO SST and the Saji et al IOD index based on the east − west SST difference are highly correlated ($r = 0.96$). The use of the latter index yields the same results.

Figure 3a shows $\sigma(T)$ in 50-yr sliding windows. Centennial modulation is obvious: $\sigma(T)$ is about 0.65°C in the first 200 years and then rises above 0.8°C from year 200 to 400. Overall $\sigma(T)$ varies between 0.6° and 0.9°C, a variation of 20% relative to the mean of 0.75°C. Here $\sigma(T)$ is correlated at −0.57 with sea surface height averaged in sliding windows, which is taken as a proxy of the thermocline depth in EEIO. The frequency of IOD occurrence is also negatively correlated with time-mean SSH (not shown), increasing as the thermocline shoals in

[1] We have also examined an extended, 2000-yr-long control run, and all the results reported in this section remain qualitatively the same.

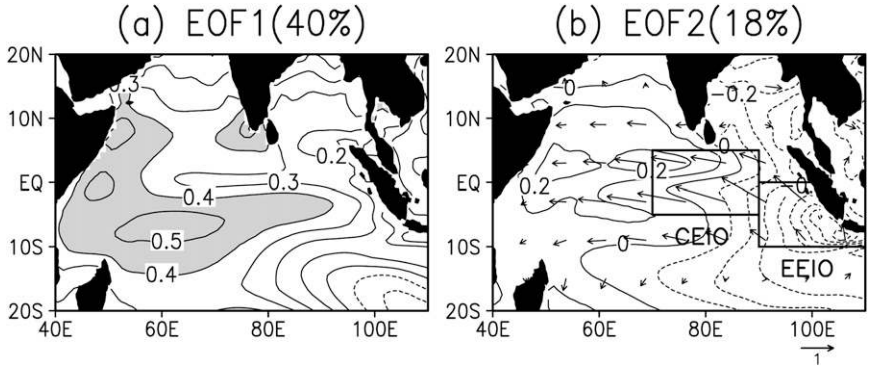

FIG. 1. (a) First and (b) second EOF modes of tropical Indian Ocean SST variability (shading >0.4°C; contours at 0.1°C intervals). Superimposed in (b) are the regressions of surface wind velocity (vectors). The boxes in (b) show the central equatorial Indian Ocean (CEIO) and EEIO.

EEIO. This relationship between SST variance and the thermocline depth in EEIO is consistent with the results from ocean model experiments in the study by Annamalai et al. (2005).

The result is also consistent with the concept of thermocline feedback. When the mean thermocline is shallow, changes in the thermocline depth and upwelling can effectively influence SST variability through entrainment. Correlation between SST and thermocline anomalies is high off the Sumatra–Java coast and southwest TIO (Xie et al. 2002), indicative of thermocline feedback. Here we measure the strength of thermocline feedback quantitatively using the SST regression upon SSH (η) in the EEIO during the August–November season, $R(T, \eta)$. Figure 3b shows $R(T, \eta)$ for interannual variability in the 50-yr sliding window. Thermocline feedback parameter $R(T, \eta)$ is highly correlated with IOD variance $\sigma(T)$. The correlation coefficient is 0.82, much higher than that between $\sigma(T)$ and mean SSH. The long-term mean value of thermocline feedback parameter is about 10°C m^{-1}. For the first 200 years, thermocline feedback is weak [$R(T, \eta)$ = 9°–10°C m^{-1}] while, for the next 200 years it rises to 11°–12°C m^{-1} as the thermocline shoals. In the model EEIO on centennial time scales, when the thermocline is shallow (deep), thermocline feedback and interannual SST variability both intensify (weaken).

The model IOD is highly correlated with ENSO during ASON (Song et al. 2007a). The correlation coefficient between SST in the EEIO and Niño-3.4 SST varies between 0.55 and 0.85, and its 50-yr sliding window

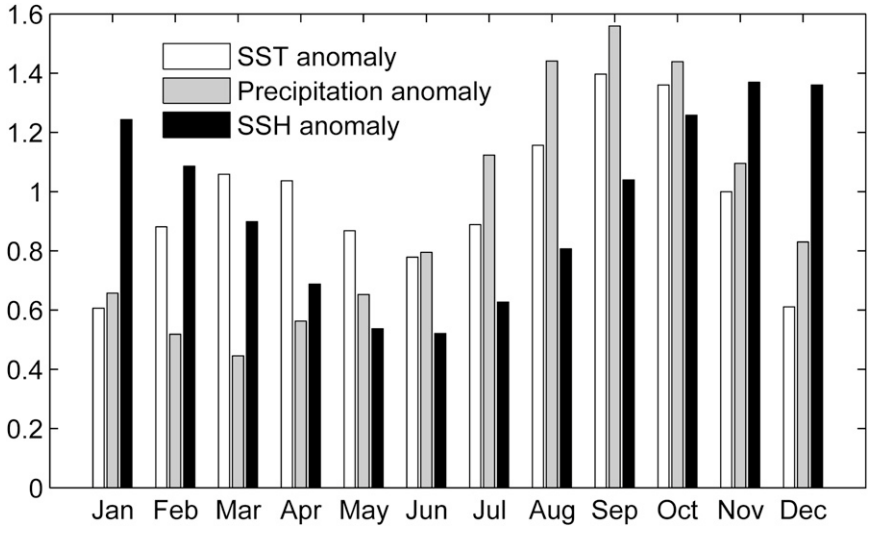

FIG. 2. Monthly standard deviations of SST, precipitation, and SSH anomalies in the EEIO normalized by their annual means.

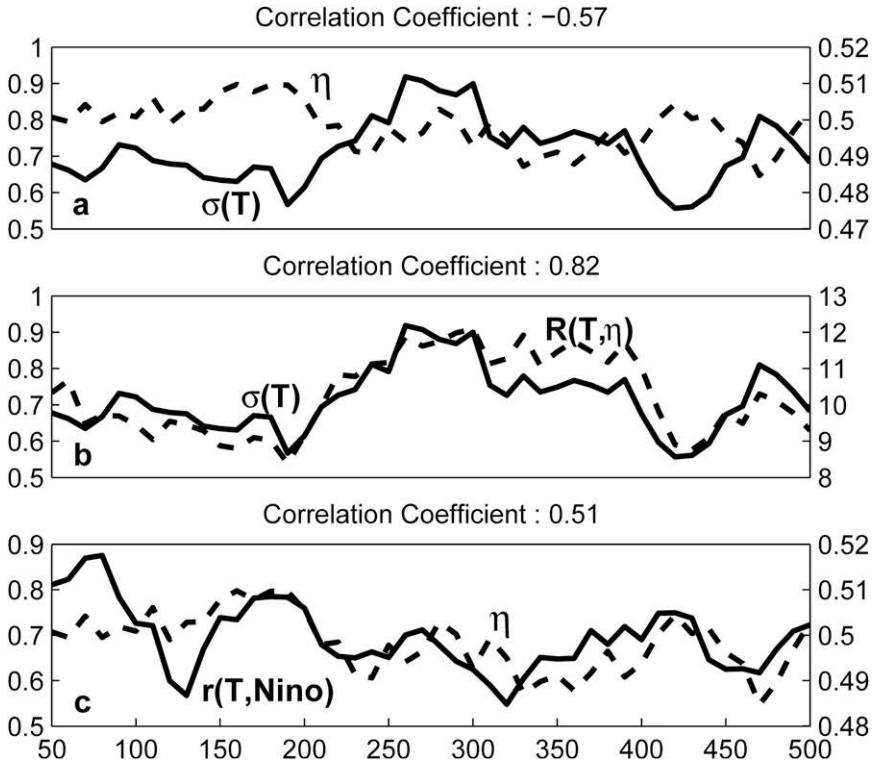

FIG. 3. Statistics in 50-yr sliding windows in the EEIO for the unforced control run: standard deviation of interannual SST variability $\sigma(T)$, SSH (η), thermocline feedback parameter $R(T, \eta)$, and SST correlation with the Niño-3.4 SST index $r(T, \text{Niño})$. All time series are averaged for ASON: (a) $\sigma(T)$ (solid line, °C) and η (dashed line, m); (b) $\sigma(T)$ (solid line, °C) and $R(T, \eta)$ (dashed line, °C m^{-1}); and (c) $r(T, \text{Niño})$ (solid line) and η (dashed line, m). Correlations between the solid and dashed curves are shown above each panel. For the extended 2000-yr simulation, the same correlations are −0.32, 0.68, and 0.38, respectively, reaching the 95% significance level ($r = 0.3$) based on t test.

index is negatively correlated with the thermocline depth in the EEIO (Fig. 3c). In a multimodel analysis, Saji et al. (2006) noted a similar relationship between the IOD–ENSO correlation and the EEIO thermocline depth. They interpreted that, when the thermocline is shallow (deep) in the EEIO, thermocline feedback is strong (weak), and the IOD is less (more) dependent on ENSO teleconnective forcing.

Thus the model IOD displays significant centennial variations in amplitude, a modulation consistent with changes in the mean thermocline depth and the strength of thermocline feedback. The cause of centennial variations in mean thermocline depth remains unclear. Chaotic IOD occurrence is one possibility, with more intense and more frequent IOD events leading to the thermocline shoaling in the EEIO (Tozuka et al. 2007). In chaotic centennial variations of the nonlinear ocean–atmosphere system, the slow thermocline shoaling and IOD intensification may be interactive, one being both cause and effect of the other.

4. IOD change in global warming

The TIO SST has been steadily increasing since the 1950s (Alory et al. 2007; Du and Xie 2008); the recent warming is part of a warming that began in the late nineteenth century (Solomon et al. 2007; Vecchi and Soden 2007b) and is projected to continue rising with increasing GHG (Vecchi and Soden 2007a). This section examines changes in the TIO mean state and IOD variability under global warming and explores their relationship, based on the CM2.1 simulations.

a. Mean state change

Figure 4 shows the change in the TIO climatology between the twenty-third and twentieth centuries for the IOD season of July–October (JASO). SST warming displays considerable spatial variations, especially in the east–west direction along the equator, amounting to 3.6°C in the northwestern equatorial Indian Ocean but dropping to just 2.4°C off the Sumatra–Java coast.

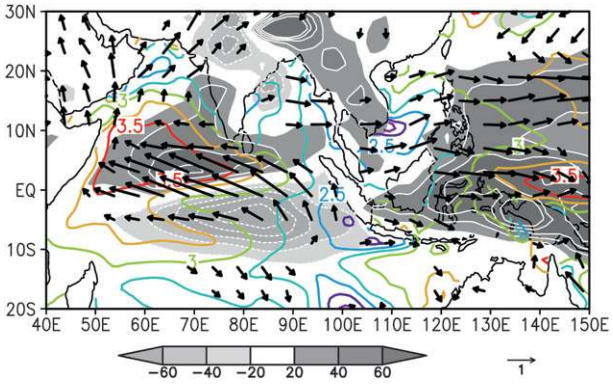

FIG. 4. The twenty-third- and twentieth-century differences in SST (contours °C), precipitation (gray shade, mm month^{-1}), and surface wind velocity (vectors, m s^{-1}) for JASO.

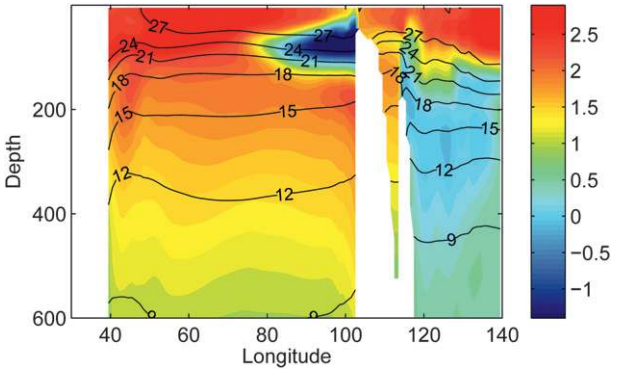

FIG. 5. The 2100–2001 difference in ocean temperature (color shading, °C) on the equator for JASO and the 2001–20 mean water temperature (contours, °C).

Associated with this SST warming pattern is a dipole of precipitation change in the TIO, positive over enhanced SST warming in the northwest basin and negative over reduced SST warming in the southeast. The SST–precipitation relation is consistent with the hypothesis of Xie et al. (2010) that SST change relative to the tropical mean warming determines changes in convective instability and tropical rainfall.

Surface wind changes are consistent with those in precipitation, SST, and the weakened Walker circulation, easterly over the equatorial Indian Ocean and westerly over the equatorial Pacific. The weakened Walker circulation is due to the muted hydrological cycle to global warming (Held and Soden 2006; Vecchi et al. 2006) as well as to the east–west gradient in TIO warming. The weakened Walker circulation changes the tropical ocean thermal structure, especially the thermocline depth on the equator. Figure 5 shows changes in seawater temperature along the equator (5°S–5°N) in the twenty-first century, a period of the most marked warming in the A1B simulation. Superimposed on a surface-intensified background structure in the vertical, the warming is substantially reduced and even reversed in sign at thermocline levels in the EEIO. This warming pattern, indicative of a thermocline shoaling, has been reported in previous studies (Vecchi and Soden 2007a; Du and Xie 2008) and likely contributes to the reduced SST warming in EEIO. Thus the patterns of climate change suggest Bjerknes feedback among east–west SST gradients, the precipitation dipole, easterly wind anomalies, and the shoaling thermocline in EEIO. Since the changes in the TIO mean state (Fig. 5) project strongly onto the interannual IOD mode, they are often called the IOD-like warming.

b. Change in interannual IOD

Under global warming, SSH rises globally owing to thermal expansion and does not represent the thermocline depth change very well. The 20°C isotherm depth deepens in response to the warming and is no longer suitable for representing the thermocline. We use the depth of maximum temperature gradient to represent the thermocline, following Vecchi and Soden (2007a). Figure 6b illustrates the change of ocean stratification in global warming in the EEIO. The dynamical thermocline as represented by the maximum temperature gradient (thick black line) tracks the layer of maximum interannual temperature variance (shading) very well. The dynamical thermocline (simply the thermocline hereafter) shoals from ~90 m in the twentieth century to ~60 m in the twenty-second century. As the EEIO thermocline shoals, thermocline feedback as measured by $R(T, \eta)$ intensifies under global warming by 20% (Fig. 7b) from ~11°C m^{-1} in the twentieth century to ~14°C m^{-1} in the twenty-second century. Analysis of extremes supports this increase in thermocline feedback. Maximum $R(T, \eta)$ is 12°C m^{-1} in the 2000-yr control run and rises to 15°C m^{-1} in global warming. Minimum $R(T, \eta)$ is typically 9°C m^{-1} in the control run and increases to 13°C m^{-1} after the late twenty-first century.

Despite the shoaling thermocline and strengthened thermocline feedback, interannual IOD variability does not change much in global warming (Fig. 7a). Throughout the A1B global warming simulation, $\sigma(T)$ varies between 0.55° and 0.8°C, a 20% variation relative to a mean of 0.69°C, much as in the unforced control run. The rather constant IOD variance under global warming is not unique to CM2.1 but rather common in the AR4 model ensemble examined by Ihara et al. (2009). Like SST, interannual precipitation variance in EEIO does not change much in time (Fig. 6a, solid line). Given the strong relationship between thermocline feedback and IOD variance in the control run, one expects that strengthened thermocline feedback under global warming

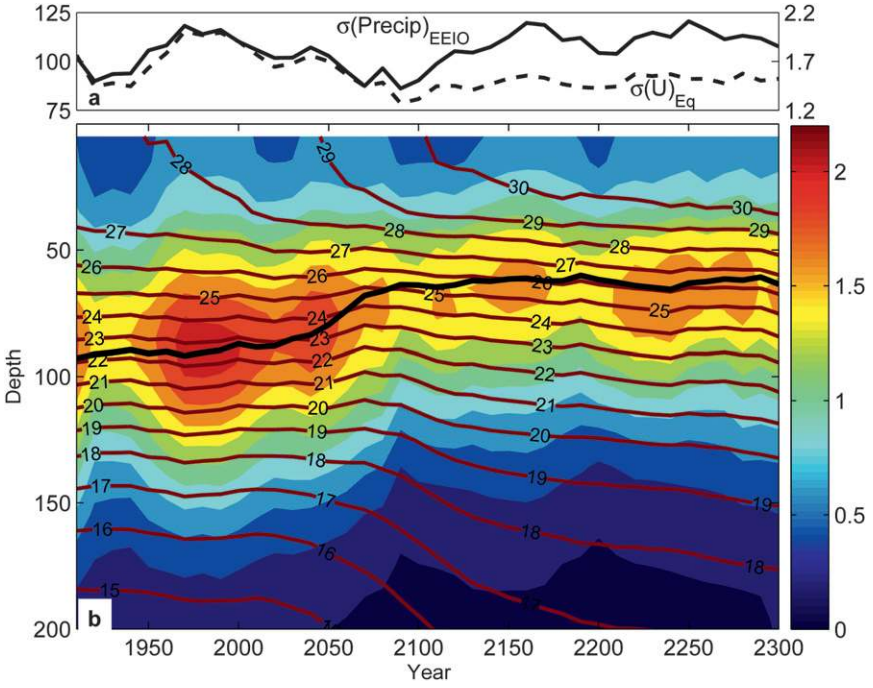

FIG. 6. Standard deviations of interannual variability for JASO in 50-yr sliding windows in the global warming run: (a) EEIO precipitation (solid line, mm month^{-1}; left axis) and zonal wind velocity in the central equatorial Indian Ocean (dashed, m s^{-1}; right axis); (b) seawater temperature in the EEIO (color shading, °C). Also shown in (b) are the thermocline (black solid line) as determined by the maximum gradient in the vertical and mean seawater temperature (°C) in brown contours.

would result in an increase in IOD variability. A puzzle arises: why does not IOD activity intensify in a warming climate as the EEIO thermocline shoals for this coupled model?

A hint to the answer lies in interannual variability in subsurface temperature in the EEIO (Fig. 6b): as the thermocline shoals in the global warming, its interannual variability decreases. A similar decrease in interannual variance is seen in zonal wind in the central equatorial Indian Ocean (5°S–5°N, 70°–90°E) (Fig. 6a, dashed line) during JASO. Zonal wind anomalies there are viewed as an integral part of Bjerknes feedback (Bjerknes 1969; Wyrtki 1975) for the interannual IOD. Therefore, we suggest that, in addition to strengthened thermocline feedback, atmospheric changes under global warming also affect interannual IOD activity. The next subsection explores this possibility.

c. *Atmospheric feedback*

Bjerknes feedback consists of oceanic as well as atmospheric feedbacks. In particular, during an IOD event, easterly wind anomalies act as a positive feedback by shoaling the thermocline and amplifying the SST cooling in the EEIO. As a measure of this atmospheric feedback, we calculate the regression of zonal wind anomalies in the central equatorial Indian Ocean (U) upon EEIO SST anomalies, $R(U, T)$. Figure 8b shows the time series of this zonal wind feedback parameter in the global warming simulation. It decreases by about 20% in global warming from 2 m s^{-1} (°C)$^{-1}$ in the twentieth century to 1.6 m s^{-1} (°C)$^{-1}$ in the twenty-second century. Similar results are obtained if the regression is calculated using SST zonal gradient defined by Saji et al. (1999) instead of EEIO SST anomalies; the regression coefficient decreases from 1.6 to 1.3 m s^{-1} (°C)$^{-1}$. This supports our hypothesis that weakened zonal wind feedback counters the effect of increased thermocline feedback. The IOD variance remains unchanged as a result.

Figure 9 shows the results from a singular value decomposition (SVD) analysis of oceanic and atmospheric fields during JASO. The oceanic (left) field is SST in the TIO (20°S–20°N, 40°–110°E), and the atmospheric (right) fields include precipitation over the TIO, zonal wind, and pressure ($\omega = dp/dt$) velocities averaged in 7.5°S–2.5°N. SVD modes are calculated separately for periods before (1861–2000) and after (2201–2300) the major GHG-induced warming. The

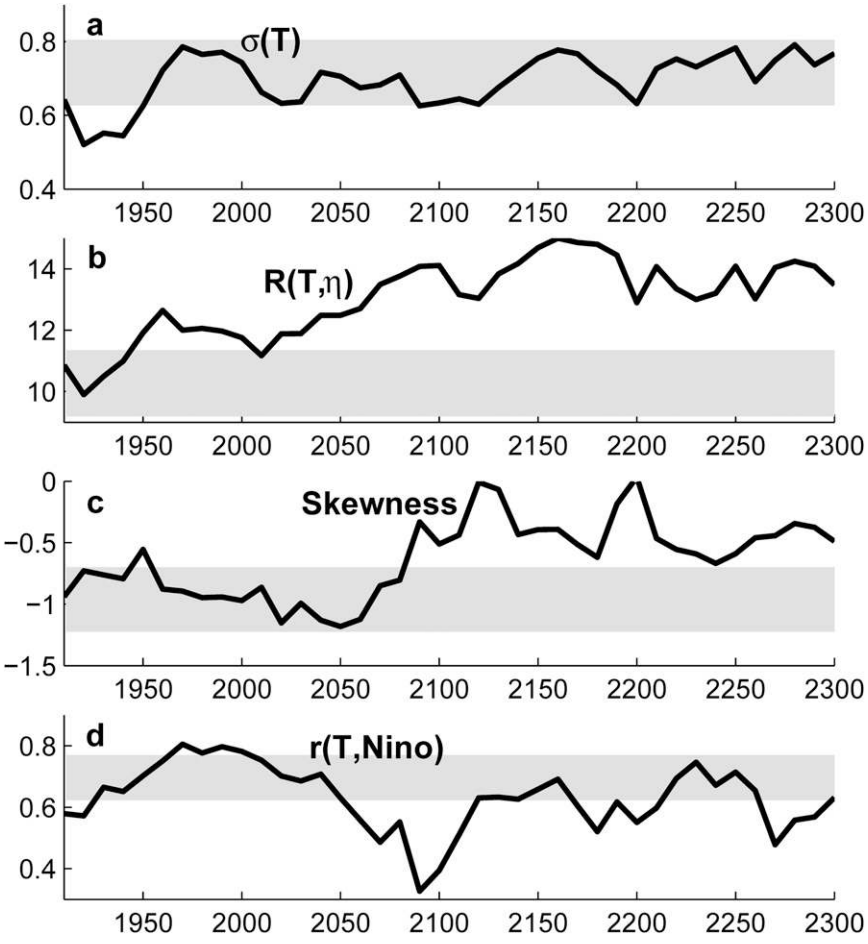

FIG. 7. Fifty-year running time series for ASON in the global warming run: (a) EEIO SST variance $\sigma(T)$ (°C), (b) thermocline feedback measured by $R(T, \eta)$ in °C m^{-1}, (c) skewness of EEIO SST variability, and (d) correlation between the Niño-3.4 and EEIO SST. Gray shade denotes the range ($\pm\sigma$) of variations in the unforced control run.

results are normalized by SST anomalies in the EEIO. For both periods, the first SVD mode is the IOD. The SST and precipitation are similar between two epochs, but the SST cooling shows a farther westward extension on the equator after global warming, a change consistent with strengthened thermocline feedback in response the shoaling thermocline in the EEIO. On the equator, the circulation anomalies are dominated by baroclinic structure. Surface easterly anomalies weaken in the after-warming epoch, reaffirming reduced atmospheric feedback.

Why then does the zonal wind feedback decrease under global warming? Dry static stability increases in the troposphere (Fig. 8a) owing to moist adiabatic adjustment in the vertical to increased surface temperature and humidity. As a measure of static stability in the midtroposphere, the potential temperature difference between 200 and 850 hPa rises steadily by 8 K, or 18%, from 42 K in 1901 to 50 K in 2300 (Fig. 8b). The increased tropospheric stability appears to hold the key to the weakened circulation response to SST anomalies (Knutson and Manabe 1995; Knutson et al. 1997). In the tropical troposphere, diabatic heating (Q) is to first order balanced by vertical temperature advection: $\omega' \partial \overline{\theta} / \partial p \sim Q'$, where θ is potential temperature and the prime and overbar denote the perturbation and mean, respectively. Recall that precipitation anomalies associated with the IOD mode do not change much in global warming (Fig. 9). In response to the same diabatic heating, increased tropospheric stability in global warming results in a weakened response in vertical velocity and baroclinic circulation in general, including zonal wind at the surface. This dynamical argument is consistent with the global warming simulation.

In global warming, atmospheric water vapor content and precipitation both increase as a global average, the

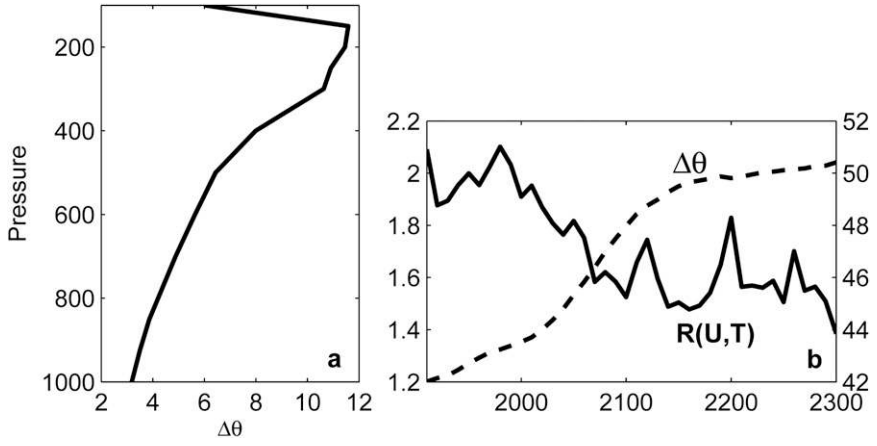

FIG. 8. (a) Twenty-third minus twentieth-century difference in potential temperature (K) averaged in the EEIO for JASO in the global warming run as a function of pressure (hPa); (b) 50-yr running time series of $\bar{\theta}|_{850\,\mathrm{hPa}}^{200\,\mathrm{hPa}}$ (dashed line, K) and zonal wind feedback parameter $R(U, T)$ (solid line, m s^{-1} K^{-1}) for JASO.

former following the Clausius–Clapeyron equation (Held and Soden 2006; Vecchi and Soden 2007a; Richter and Xie 2008). On regional scales, precipitation may increase or decrease in global warming. Over the tropical Indian Ocean, specifically, precipitation increases (decreases) in the northwestern (southeastern) basin (Fig. 4). The basin mean is nearly unchanged. As a result, precipitation response to IOD remains constant (Fig. 6a), and

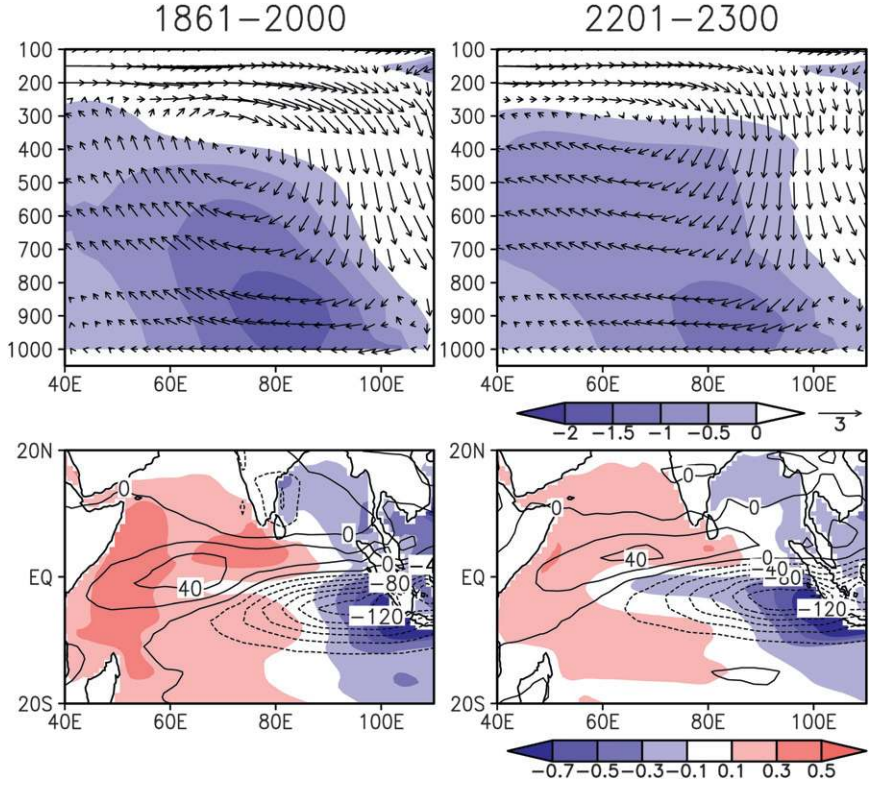

FIG. 9. First SVD mode between SST (color shading in bottom panel, °C) and atmospheric fields including precipitation (contours in bottom, mm month^{-1}) over the TIO, zonal (shading in top, m s^{-1}) and vertical velocities (in Pa s^{-1}, vectors with zonal velocity) averaged in 5°S–5°N for ASON during (left) 1861–2000 and (right) 2201–2300.

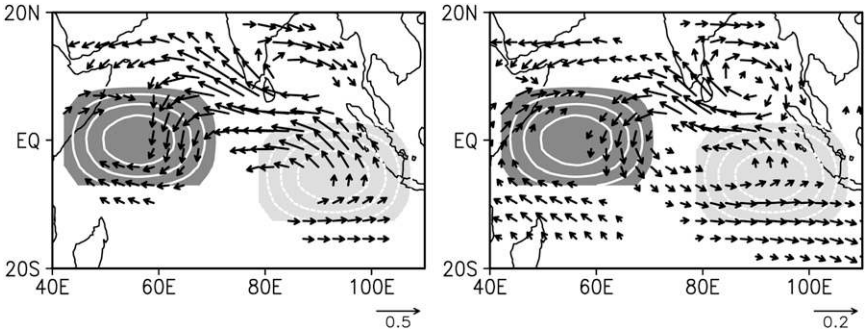

FIG. 10. Linear atmospheric model wind response at 900 hPa (vector, m s^{-1}) to a prescribed dipolar heating pattern for the mean states of (left) 1861–2000 and (right) 2201–2300. Diabatic heating rate at 500 hPa is shown in grade shade (dark >0.1 and light <−0.1 K day^{-1}; white contours at 0.1 K day^{-1} intervals).

the tropospheric stability effect dominates atmospheric feedback change.

d. LBM

To test the atmospheric stability effect on zonal wind feedback, we conduct experiments with a dry linear baroclinic model (LBM), forced by prescribed diabatic heating. In the vertical, the heating is confined between 900 and 100 hPa with a peak at 500 hPa to mimic condensational heat release in deep convection. It is made of horizontally confined components in the following function of longitude (x) and latitude (y):

$$Q = \begin{cases} Q_0 \sin\pi\left[\dfrac{(x - X_W)}{(X_E - X_W)}\right] \sin\pi\left[\dfrac{(y - Y_S)}{(Y_N - Y_S)}\right] & \text{for } X_W < x < X_E, \quad Y_S < y < Y_N \\ 0, \text{elsewhere} \end{cases} . \tag{1}$$

We place a positive heating in the western (X_W = 50°E, X_E = 70°E, Y_S = 5°S, Y_N = 5°N) and a negative heating in the eastern (X_W = 90°E, X_E = 110°E, Y_S = 10°S, Y_N = 0°) equatorial Indian Ocean. The maximum heating rate is set at 1 K day^{-1} (−1 K day^{-1}) for the positive (negative) poles. We make two runs with the same heating distribution using the CM2.1 September mean states for the twentieth (1861–2000) and twenty-third (2201–2300) centuries, respectively. Each experiment lasts 30 days, reaching a steady state.

The LBM simulation under the twentieth-century mean state captures many surface wind features important for IOD (left panel of Fig. 10). Easterly wind anomalies appear along the equator, acting to shoal the thermocline in the east. There is an anticyclonic anomalous circulation in the southeast TIO with the southeasterlies favorable for upwelling on the Sumatra coast.

The LBM simulation for the twenty-third century is similar to that for the twentieth century, albeit with reduced magnitude. The right panel of Fig. 10 illustrates the difference in the response to the heating anomalies between twentieth and twenty-third centuries. The difference is nearly identical to the twentieth-century simulation, indicating that the surface wind response weakens by 30%–40% in the twenty-third century. Thus the LBM results support the hypothesis that, in global warming, increased tropospheric stability weakens the zonal wind feedback for the IOD.

5. IOD skewness

The positive phase of IOD is associated with SST cooling in the EEIO and easterly wind anomalies in the central basin. The IOD is highly asymmetric between the positive and negative phases with the former much larger in amplitude (e.g., Hong et al. 2008). The standard deviation of ASON-mean SST in EEIO is 0.49 (0.3) for negative (positive) anomalies. The negative extreme is −2.5°C and the positive one is less than 1.5°C for the 500-yr control run.

Figure 11 shows the scatter diagram of SST and SSH over the EEIO for ASON. SST and SSH anomalies are highly correlated at r = 0.86. The SST–SSH relationship is not linear. The SST/SSH slope is much steeper for negative than positive anomalies, indicating a stronger thermocline feedback for EEIO cooling events. The stronger thermocline feedback in turn appears to be

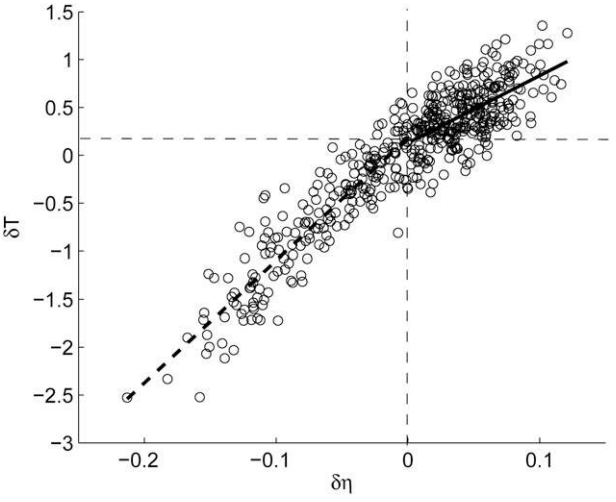

FIG. 11. Scatter diagram for interannual anomalies of SSH (η, m) and SST (°C) in the EEIO for ASON. The solid and dashed lines denote the linear regressions for positive and negative SSH anomalies, respectively.

the cause of asymmetry between positive and negative phases of IOD. Compared to the eastern Pacific and Atlantic, the thermocline in the EEIO is deep—more conducive to thermocline feedback for negative than positive thermocline depth anomalies. Thus we suggest that the deep mean thermocline is the ultimate cause of asymmetry in thermocline feedback and IOD between its phases.

We measure this asymmetry with the skewness of EEIO SST anomalies.[2] Figure 7c shows the change in SST skewness in the 400-yr global warming simulation. For the first 150 years, the skewness is strongly negative, indicating stronger cold than warm events in EEIO. In the second half of the twenty-first century, the negative skewness decreases by more than 30% from −1 to −0.5 and remains low. This skewness change is consistent with the above hypothesis that a relatively deep mean thermocline in the EEIO causes the SST skewness. As global warming forces the EEIO thermocline to shoal (Fig. 7), thermocline feedback not only becomes stronger than in current climate but also is more symmetric between cold and warm events (Figs. 7b,c).

Unlike global warming in which the SST skewness weakens in response to a shoaling thermocline, centennial variations in SST skewness in the unforced control run are not significantly correlated with in the thermocline depth in EEIO (not shown), indicating that the latter are not the cause of the former. It is likely that centennial variations in the control run are chaotic in nature, originating from nonlinearity of the coupled ocean–atmosphere system (e.g., Timmermann and Jin 2003). There might even be a positive feedback in the chaotic vacillations: because of the negative skewness, increased IOD activity leads to a decrease in the mean thermocline depth, which in turn helps strengthen thermocline feedback and IOD activity (Figs. 3a,b). The lack of coherent variations in skewness is consistent with this negative feedback: increased IOD activity is accompanied by high skewness and thermocline shoaling, in turn, would weaken skewness. The net of the opposing effects due to a shoaling thermocline and enhanced IOD variability appears small on skewness.

6. Summary

We have investigated unforced low-frequency modulation of and GHG-forced change in the interannual IOD mode using the GFDL coupled model CM2.1. IOD variability displays distinct changes in the unforced and forced simulations. In the unforced control run, IOD variance $\sigma(T)$ exhibits multicentennial variations of 20% in amplitude. In the centennial modulation, IOD activity intensifies when the mean thermocline shoals in the EEIO. We use a regression method to measure thermocline feedback. In the EEIO, the thermocline shoaling strengthens thermocline feedback, leading to elevated IOD variability.

In global warming, the thermocline in the EEIO shoals from 90 to 60 m with easterly wind anomalies on the equator, the latter associated with the slowdown of the Walker circulation. While the shoaling thermocline increases thermocline feedback by 20%, peculiarly, IOD variance does not change much in global warming. Our analysis reveals that the zonal wind response to IOD SST anomalies weakens by 20% as tropospheric static stability increases in global warming. Our LBM experiments confirm that increased tropospheric stability reduces the atmospheric circulation response to a SST dipole. The weakened atmospheric feedback reflects in reduced zonal wind variance in the central equatorial Indian Ocean and decreased subsurface temperature variance. Thus it is because the reduced zonal wind feedback opposes the increased thermocline feedback that IOD variance remains largely unchanged in global warming (Fig. 12). Theses changes in atmosphere–ocean feedbacks can be traced back to robust changes in the mean state, specifically the thermocline shoaling in the EEIO and increased atmospheric stratification.

While the IOD second moment (variance) does not change, its third moment (skewness) weakens significantly

[2] The skewness is defined as $m_3/(m_2)^{3/2}$, where $m_k = \sum_{i=1}^{N}(x_i - \overline{X})^k/N$ is the kth moment and x_i is the ith datum, $\overline{X}$ the climatological mean, and N the length of the data.

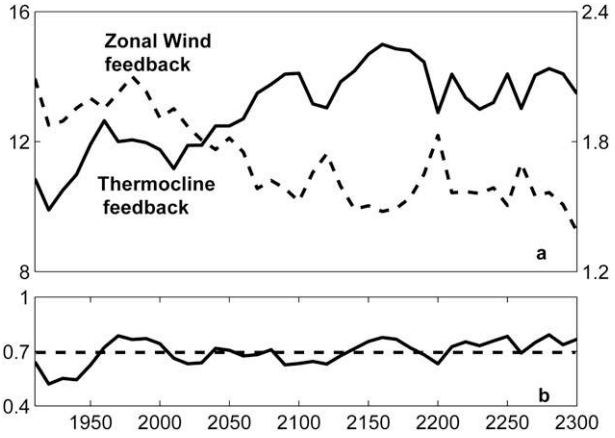

FIG. 12. Fifty-year running time series for ASON in the global warming run: (a) thermocline [$R(T, \eta)$ in solid, °C m^{-1}] and zonal wind [$R(U, T)$ dashed, m s^{-1} K^{-1}] feedback parameters in the EEIO; (b) standard deviation (°C) of interannual SST variability in EEIO.

in global warming. The IOD is strongly skewed in the control run toward cooling events in the EEIO. We interpret that IOD skewness originates from the relatively deep thermocline in the EEIO, which favors cold over warm events for thermocline feedback. In global warming, as the thermocline shoals over the EEIO, thermocline feedback is more equally applied to anomalies of both signs than in the current climate, leading to a weakened skewness.

The present study focuses on changes in ocean–atmospheric feedbacks internal to the TIO, and the results appear to explain IOD behavior in both free and forced simulations. The model IOD is correlated with ENSO, and ENSO change under global warming is an additional source of IOD change. In CM2.1, ENSO does not change much in amplitude (Guilyardi et al. 2009) in global warming—neither does its correlation with IOD (Fig. 7d). If anything, the ENSO–IOD correlation seems to decrease slightly in a warmer climate, especially during the late twenty-first and early twenty-second centuries. This decrease in ENSO forcing of IOD is consistent with the strengthened thermocline feedback, which allows the IOD to develop more independently of ENSO (Saji et al. 2006).

Abram et al. (2008) reported a recent intensification of the IOD based on coral records for the past 150 years. The IOD was weak in the late nineteenth and early twentieth centuries and then strengthened since 1920. Their analysis also suggested TIO changes such as anomalous easterly winds, SST cooling, and reduced precipitation in the EEIO, features consistent with our coupled model projection. In CM2.1, however, thermocline shoaling in the EEIO does not lead to intensified IOD activity, as the strengthened thermocline feedback is opposed by reduced zonal wind feedback. Thus, our results suggest that the recent IOD intensification is likely part of natural low-frequency modulation instead of global warming. We call for caution in relying on model projections to interpret observations. While the IOD-like pattern is projected in many global warming simulations (Vecchi and Soden 2007a; Du and Xie 2008; Meng et al. 2010, manuscript submitted to *Adv. Atmos. Sci.*), there is at least one study suggesting that TIO climate change displays a negative IOD-like pattern in equatorial winds and thermocline adjustment (Trenary and Han 2008). Sustained observations and improved physical understanding are necessary to reduce uncertainties in attributing observed climate change and projecting future change.

Acknowledgments. The authors would like to acknowledge helpful suggestions from two anonymous reviewers. Much of the work was performed when X.T.Z. was a visiting student at the International Pacific Research Center on a Chinese Ministry of Education oversea scholarship. This work is supported by the Natural Science Foundation of China 40830106 and the 111 Project under Grant B07036, the Changjiang Scholar Program of the Chinese Ministry of Education, the U.S. National Science Foundation, and the Japan Agency for Marine-Earth Science and Technology.

REFERENCES

Abram, N. J., M. K. Gagan, J. E. Cole, W. S. Hantoro, and M. Mudelsee, 2008: Recent intensification of tropical climate variability in the Indian Ocean. *Nat. Geosci.,* **1,** 849–853.

Alory, G., S. Wijffels, and G. Meyers, 2007: Observed temperature trends in the Indian Ocean over 1960–1999 and associated mechanisms. *Geophys. Res. Lett.,* **34,** L02606, doi:10.1029/2006GL028044.

An, S.-I., J.-S. Kug, Y.-G. Ham, and I.-S. Kang, 2008: Successive modulation of ENSO to the future greenhouse warming. *J. Climate,* **21,** 3–21.

Annamalai, H., J. Potemra, R. Murtugudde, and J. P. McCreary, 2005: Effect of preconditioning on the extreme climate events in the tropical Indian Ocean. *J. Climate,* **18,** 3450–3469.

Ashok, K., W.-L. Chan, T. Motoi, and T. Yamagata, 2004: Decadal variability of the Indian Ocean dipole. *Geophys. Res. Lett.,* **31,** L24207, doi:10.1029/2004GL021345.

Behera, S. K., J.-J. Luo, and T. Yamagata, 2008: Unusual IOD event of 2007. *Geophys. Res. Lett.,* **35,** L14S11, doi:10.1029/2008GL034122.

Bjerknes, J., 1969: Atmospheric teleconnections from the equatorial Pacific. *Mon. Wea. Rev.,* **97,** 163–172.

Capotondi, A., A. Wittenberg, and S. Masina, 2006: Spatial and temporal structure of tropical Pacific interannual variability in 20th century coupled simulations. *Ocean Modell.,* **15,** 274–298.

Chang, P., and Coauthors, 2006: Climate fluctuations of tropical coupled system—The role of ocean dynamics. *J. Climate,* **19,** 5122–5174.

Collins, M., 2005: El Niño- or La Niña-like climate change? *Climate Dyn.,* **24,** 89–104.

Delworth, T. L., and Coauthors, 2006: GFDL's CM2 global coupled climate models. Part I: Formulation and simulation characteristics. *J. Climate,* **19,** 643–674.

Deser, C., A. S. Phillips, and J. W. Hurrell, 2004: Pacific interdecadal climate variability: Linkages between the tropics and the North Pacific during boreal winter since 1900. *J. Climate,* **17,** 3109–3124.

Du, Y., and S.-P. Xie, 2008: Role of atmospheric adjustments in the tropical Indian Ocean warming during the 20th century in climate models. *Geophys. Res. Lett.,* **35,** L08712, doi:10.1029/2008GL033631.

——, ——, G. Huang, and K. Hu, 2009: Role of air–sea interaction in the long persistence of El Niño–induced north Indian Ocean warming. *J. Climate,* **22,** 2023–2038.

Fedorov, A. V., and S. G. Philander, 2000: Is El Niño changing? *Science,* **288,** 1997–2002.

GFDL Global Atmospheric Model Development Team, 2004: The new GFDL global atmosphere and land model AM2–LM2: Evaluation with prescribed SST simulations. *J. Climate,* **17,** 4641–4673.

Griffies, S., M. J. Harrison, R. C. Pacanowski, and A. Rosati, 2003: A technical guide to MOM4. GFDL Ocean Group Tech. Rep. 5, NOAA/Geophysical Fluid Dynamics Laboratory, 295 pp.

Guilyardi, E., A. Wittenberg, A. Fedorov, M. Collins, C. Wang, A. Capotondi, G. J. van Oldenborgh, and T. Stockdale, 2009: Understanding El Niño in ocean–atmosphere general circulation models: Progress and challenges. *Bull. Amer. Meteor. Soc.,* **90,** 325–340.

Held, I. M., and B. J. Soden, 2006: Robust responses of the hydrological cycle to global warming. *J. Climate,* **19,** 5686–5699.

Hong, C.-C., T. Li, LinHo, and J.-S. Kug, 2008: Asymmetry of the Indian Ocean dipole. Part I: Observational analysis. *J. Climate,* **21,** 4834–4848.

Ihara, C., Y. Kushnir, and M. A. Cane, 2008: Warming trend of the Indian Ocean SST and Indian Ocean dipole from 1880 to 2004. *J. Climate,* **21,** 2035–2046.

——, ——, ——, and H. P. Victor, 2009: Climate change over the equatorial Indo-Pacific in global warming. *J. Climate,* **22,** 2678–2693.

Klein, S. A., B. J. Soden, and N.-C. Lau, 1999: Remote sea surface temperature variations during ENSO: Evidence for a tropical atmospheric bridge. *J. Climate,* **12,** 917–932.

Knutson, T. R., and S. Manabe, 1995: Time-mean response over the tropical Pacific to increased CO_2 in a coupled ocean–atmosphere model. *J. Climate,* **8,** 2181–2199.

——, ——, and D. Gu, 1997: Simulated ENSO in a global coupled ocean–atmosphere model: Multidecadal amplitude modulation and CO_2 sensitivity. *J. Climate,* **10,** 138–161.

Lin, S.-J., 2004: A ''vertically Lagrangian'' finite-volume dynamical core for global models. *Mon. Wea. Rev.,* **132,** 2293–2307.

Luo, J. J., S. K. Behera, Y. Masumoto, H. Sakuma, and T. Yamagata, 2008: Successful prediction of the consecutive IOD in 2006 and 2007. *Geophys. Res. Lett.,* **35,** L14S02, doi:10.1029/2007GL032793.

Meehl, G. A., G. W. Branstator, and W. M. Washington, 1993: Tropical Pacific interannual variability and CO_2 climate change. *J. Climate,* **6,** 42–63.

Murtugudde, R., J. P. McCreary, and A. J. Busalacchi, 2000: Oceanic processes associated with anomalous events in the Indian Ocean with relevance to 1997–1998. *J. Geophys. Res.,* **105,** 3295–3306.

Richter, I., and S.-P. Xie, 2008: Muted precipitation increase in global warming simulations: A surface evaporation perspective. *J. Geophys. Res.,* **113,** D24118, doi:10.1029/2008JD010561.

Saji, N. H., B. N. Goswami, P. N. Vinayachandran, and T. Yamagata, 1999: A dipole mode in the tropical Indian Ocean. *Nature,* **401,** 360–363.

——, S.-P. Xie, and T. Yamagata, 2006: Tropical Indian Ocean variability in the IPCC twentieth-century climate simulations. *J. Climate,* **19,** 4397–4417.

Schott, F. A., S.-P. Xie, and J. P. McCreary, 2009: Indian Ocean circulation and climate variability. *Rev. Geophys.,* **47,** RG1002, doi:10.1029/2007RG000245.

Solomon, S., D. Qin, M. Manning, M. Marquis, K. Averyt, M. M. B. Tignor, H. L. Miller Jr., and Z. Chen, Eds., 2007: *Climate Change 2007: The Physical Science Basis*. Cambridge University Press, 996 pp.

Song, Q. N., G. A. Vecchi, and A. Rosati, 2007a: Indian Ocean variability in the GFDL CM2 coupled climate model. *J. Climate,* **20,** 2895–2916.

——, ——, and ——, 2007b: The role of the Indonesian Throughflow in the Indo–Pacific climate variability in the GFDL Coupled Climate Model. *J. Climate,* **20,** 2434–2451.

Timmermann, A., and F.-F. Jin, 2003: A nonlinear theory for El Niño bursting. *J. Atmos. Sci.,* **60,** 152–165.

——, J. Oberhuber, A. Bacher, M. Esch, M. Latif, and E. Roeckner, 1999: Increased El Niño frequency in a climate model forced by future greenhouse warming. *Nature,* **398,** 694–697.

Tozuka, T., J. J. Luo, S. Masson, and T. Yamagata, 2007: Decadal modulations of the Indian Ocean Dipole in the SINTEX-F1 coupled GCM. *J. Climate,* **20,** 2881–2894.

Trenary, L. L., and W. Han, 2008: Causes of decadal subsurface cooling in the tropical Indian Ocean during 1961–2000. *Geophys. Res. Lett.,* **35,** L17602, doi:10.1029/2008GL034687.

van Oldenborgh, G. J., S. Philip, and M. Collins, 2005: El Niño in a changing climate: A multi-model study. *Ocean Sci.,* **1,** 81–85.

Vecchi, G. A., and B. J. Soden, 2007a: Global warming and the weakening of the tropical circulation. *J. Climate,* **20,** 4316–4340.

——, and ——, 2007b: Effect of remote sea surface temperature change on tropical cyclone potential intensity. *Nature,* **450,** 1066–1070.

——, ——, A. T. Wittenberg, I. M. Held, A. Leetmaa, and M. J. Harrison, 2006: Weakening of tropical Pacific atmospheric circulation due to anthropogenic forcing. *Nature,* **441,** 73–76.

Watanabe, M., and M. Kimoto, 2000: Atmosphere-ocean thermal coupling in the North Atlantic: A positive feedback. *Quart. J. Roy. Meteor. Soc.,* **126,** 3343–3369.

Webster, P. J., A. M. Moore, J. P. Loschnigg, and R. R. Leben, 1999: Coupled ocean–atmosphere dynamics in the Indian Ocean during 1997–98. *Nature,* **401,** 356–360.

Wittenberg, A. T., A. Rosati, N.-C. Lau, and J. J. Ploshay, 2006: GFDL's CM2 global coupled climate models. Part III: Tropical Pacific climate and ENSO. *J. Climate,* **19,** 698–722.

Wyrtki, K., 1975: El Niño—The dynamic response of the equatorial Pacific Ocean to atmospheric forcing. *J. Phys. Oceanogr.,* **5,** 572–584.

Xie, S.-P., H. Annamalai, F. A. Schott, and J. P. McCreary, 2002: Structure and mechanisms of south Indian Ocean climate variability. *J. Climate,* **15,** 864–878.

——, C. Deser, G. A. Vecchi, J. Ma, H. Teng, and A. T. Wittenberg, 2010: Global warming pattern formation: Sea surface temperature and rainfall. *J. Climate,* **23,** 966–986.

Yamagata, T., S. K. Behera, J.-J. Luo, S. Masson, M. Jury, and S. A. Rao, 2004: Coupled ocean–atmosphere variability in the tropical Indian Ocean. *Earth Climate: The Ocean–Atmosphere Interaction, Geophys. Monogr.,* Vol. 147, Amer. Geophys. Union, 189–212.

Yuan, D., and W. Han, 2006: Roles of equatorial waves and western boundary reflection in the seasonal circulation of the equatorial Indian Ocean. *J. Phys. Oceanogr.,* **36,** 930–944.